


## Article

# Analysis of the Incidence of Direct Lightning over a HVDC Transmission Line through EFD Model

Ednardo Rodrigues <sup>1,\*</sup>, Ricardo S. T. Pontes <sup>1,2</sup>, João Bandeira <sup>1</sup> and Victor P. B. Aguiar <sup>3,†</sup> 

<sup>1</sup> Department of Electrical Engineering, Federal University of Ceará (UFC), Fortaleza, Ceará 60440-900, Brazil; ricthe@unifor.br (R.S.T.P.); joaohlb@hotmail.com (J.B.)

<sup>2</sup> Center of Technologic Sciences, University of Fortaleza (Unifor), Fortaleza, Ceará 60811-905, Brazil

<sup>3</sup> Department of Engineering and Technology, Federal Rural University of Semi-Arid Region (UFERSA), Mossoró 59625-900, Rio Grande do Norte, Brazil; victor@ufersa.edu.br

\* Correspondence: ednardorodrigues@dee.ufc.br

† This author is a member of IEEE.

Received: 9 January 2019; Accepted: 4 February 2019; Published: 11 February 2019



**Abstract:** HVDC systems are becoming more common worldwide, specially in Brazil, since the adoption of such system for Itaipu's hydroelectric complex in the 1980's. Today, the country has the Xingu-Estreito bipole, with length of 2375 km. This system crosses a region with high lightning incidence, a phenomenon which causes faults in power systems. The most widely used model for the positioning of the arrestor cables over a transmission line is the electrogeometric model. This model, however, does not take into account the different potentials over the structure's surface, and therefore presents significant inaccuracies when assessing the risk of lightning strikes on structures such as a HVDC line. This work then used the Electric Field Deflection (EFD) model with the aid finite elements. Four levels of lightning are assessed (I, II, III and IV), with current peaks of 3.9, 5.4, 10.1 and 15.7 kA. It was verified that the positive pole tends to attract most of the lightning with shielding failures width (SFW) of 12, 8, 4 and 0 m. It was then proposed to move the arrestor cables horizontally. The study indicates that this horizontal shifting of the cables in 5 and 8 m toward the side with larger chance of direct incidence reduces the shielding failure widths in 50% for peak current of 3.9 kA and almost eliminates the strikes for lightning with peak currents of 5.4, 10.1 and 15.7 kA.

**Keywords:** HVDC; EFD; lightning, transmission line; LPS

## 1. Introduction

The introduction of new energy sources to the classically thermal and hydroelectric power grid brings the necessity of more flexible alternatives to ensure the best performance of large-scale power transmission [1,2]. In large systems, such as the ones that extend over countries with large territories, like those of Brazil, India, China and the USA, this need is being met through the use of High Voltage Direct Current (HVDC) transmission lines [1,2].

It is common knowledge that a strong commercial dispute over the hegemony of the generation, transmission and distribution of electricity to the general population took place. This dispute, referred to as “war of the currents” in history and popular culture, reached its peak during the 1880's and 1890's and was championed on one side by Thomas Edison, proponent of direct current systems and, on the other side, by George Westinghouse, advocate of alternate current systems [3]. After great commercial dispute, which involved discussions about electric safety, alternate current systems dominated the electricity transmission sector with high voltages of around 150 kV [4].

The predominance of alternate current systems can be attributed mainly to the advent of electric transformers, developed commercially by William Stanley, which enable an easy conversion of

voltage levels in alternate current [3]. The use of high voltage brought technical and economic benefits due to reduced transmission losses and lower conductor material costs [3–5]. In addition, the development of the induction motor, by Nikola Tesla, allowed alternate current systems to be extended to industrial applications [6].

Although alternate current has widely dominated the market, it presents some disadvantages, specially when the connection of systems with different frequencies is required. In these cases, direct current systems bring advantages. For this reason, direct current technologies now tend to be integrated to power systems, in addition to alternate current, in order to achieve optimized designs. According to [7], engineer René Thury, in 1889, started developing a transmission system which integrated both direct and alternate current technologies. Thury's system used electrical machines in the connection between two systems to perform the electromechanic energy conversion that allowed the coexistence of Alternate Current (AC) and Direct Current (DC) in a same power grid.

This idea would be the starting point for the later development of HVDC systems. For a long period, the static conversion between AC and DC was prohibitively expensive, and this technology was turned down in favour of purely AC systems [8]. After the development of semiconductor technologies and the resulting replacement of vacuum tubes for static semiconductor switches, interest in interconnecting AC and DC systems has been revived. HVDC transmission systems have been spreading worldwide since its first commercial deployment in 1954 [9]. Since then, these technologies have been perfected and gaining larger applicability. There are currently more than 200 HVDC systems in operation worldwide and technological advances continue to arise [10].

Brasil's electricity generation and transmission grid is a large-scale hydro-thermal-wind power system, with predominance of hydroelectric plants and multiple owners, currently facing large insertion of renewable sources, which make it one of the world's cleanest energy grids [11]. This system is virtually entirely interconnected and constitutes the "*Sistema Integrado Nacional*" (SIN) (or "National Integrated System" in english), which is composed of four subsystems: South, Southeast/Central-West, North and Northeast, which are interconnected through the transmission grid, enabling the transfer of power between these subsystems and allowing for synergy gains through the diversity between hydrologic regimes of the many hydrographic basins present in the country's territory [12].

With a prominent position in the use of HVDC technology, Brazil plays a key role in the development of such systems. The country was pioneer in the use of  $\pm 600$  kV voltage in the design of the transmission of part of the electricity generated in Itaipu hydropower plant [13]. Itaipu hydropower plant, as a binational unit with participation of Brasil and Paraguay, represents a generation unit with different output frequencies, according to the nominal frequency of each country's grid, with half of the generation in 50 Hz and the other half in 60 Hz. The necessity of transferring the electricity surplus of the 50 Hz side to the consumer center in the region of São Paulo, which operates in 60 Hz, prompted the use of a HVDC transmission technology.

Itaipu's project, which was once the world's largest HVDC system, consists of two bipoles with total capacity of 6300 MW, with operations beginning in October 1984 (1st bipole), initially at  $\pm 300$  kV. After nine months of operation, in July 1985, the voltage level was elevated to  $\pm 600$  kV, and the second bipole was inaugurated in 1987. In addition to the need of asynchronous integration, another reason that led to the adoption of the HVDC topology was the transmission distance. The transmission lines have length of 785 and 805 km, and the use of DC has proven itself more cost-effective for such distances [2].

Since its first implementation, in Itaipu, HVDC has been proven to be successful. New projects have been implemented since then. Table 1 illustrates some characteristics of HVDC projects in Brazil. Beginning in 2005, the studies for the interconnection of the power plants of Jirau and Santo Antônio, both along the Madeira river, in the state of Rondônia, Amazon rainforest, indicate the alternative with lower global cost as being a 2 bipole,  $\pm 600$  kV HVDC design. Later, in 2007, a new study proposed, as a second alternative, the possibility of AC transmission. At the auction execution permit for the Madeira river complex's project, at last, 2 alternatives were proposed. The first was one with

one DC bipole and two AC lines at 500 kV. The second, which was the winning one, consisted of 2 DC bipoles, each to transmit 3150 MW at  $\pm 600$  kV [14].

**Table 1.** HVDC projects in Brazil (2018).

Project	Power (MW)	Voltage Level (kV)	Location	Line Length (km)	Technology	Year
Itaipu 1	3150	600	PR-SP	785	LCC bipolar	1984
Itaipu 2	3150	600	PR-SP	805	LCC bipolar	1987
Garabi	$2 \times 1100$	70	Garabi, RS	-	CCC back-to-back	2000–2002
Rio Madeira	$2 \times 3150$	600	RO-SP	2375	LCC bipolar	2013
Belo Monte 1	2000	800	PA-MG	2100	LCC bipolar	2017
Belo Monte 2	2000	800	PA-RJ	2518	LCC bipolar	2020

Another important HVDC application in Brazil can be seen at Belo Monte's hydropower complex, which represents the maintenance of clean, sustainable and reliable electric grid that, along with other energy sources, places Brazil in a privileged position in the global scenario [15]. Belo Monte's plant, with installed capacity of 11233 MW, increased the necessity of interconnection for the balancing of electricity's generation and consumption between the country's subsystems. A big challenge to this is the fact the the referred power plant, located in the Amazon rainforest, is more than 2000 km away from the country's centers of consumption. Studies of technical and economical feasibility for the construction of two HVDC transmission lines for the interconnection of these two subsystems (North and Southeast) were carried out in order to solve this issue.

Belo Monte's transmission system, which transmits energy from North to Southeast Brazil, makes use of a 800 kV DC scheme. Said system was designed to comprise two DC bipoles. The first one, devised to interconnect the substations (SS) of Xingu (state of Pará) and Estreito (state of Minas Gerais), has a length of 2375 km. The second one, with length of approximately 2500 km, intends to interconnect the substations Xingu and Terminal Rio (state of Rio de Janeiro), but its operation should start only in 2020.

The design for Bipole 1 comprises the following elements:

- AC/DC Converting Station, 500 kV/ $\pm 800$  kV, 4000 MW (SS Xingu).
- AC/DC Converting Station, 500 kV/ $\pm 800$  kV, 3850 MW (SS Estreito).
- HVDC line at  $\pm 800$  kV (Xingu – Estreito).

According to [16], transmission line Xingu - Estreito presents the physical characteristics included in Table 2. As it can be verified, transmission line Xingu - Estreito is lengthy, stretching almost 2400 km, and interconnects two geographic regions completely distinct in terms of climate and environmental aspects. Under these conditions, the lines are vulnerable to lightning. In these regions, cloud to ground lightning density ( $N_g$ ) is between 5 and 6 discharges/km<sup>2</sup>/year. In Brazil,  $N_g$  varies from 0.1 to 18 lightning/km<sup>2</sup>/year throughout its whole territory [17].

Lightning Protection Systems (LPS) have been revised by many researchers [18–20]. The models used to determine the positioning of the captors on a LPS are called incidence models. The most widely used model for transmission lines is the electrogeometric [21]. The electrogeometric model, however, does not take into account the different potentials that can exist along the surface of the structure, as in the case of DC transmission lines.

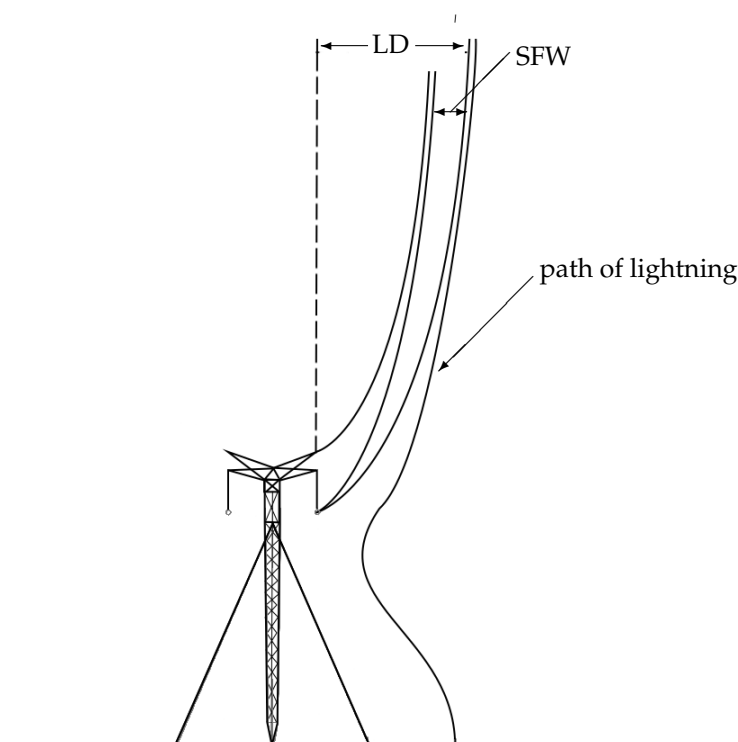
This work proposes an analysis of the LPS of the HVDC line between Belo Monte and Estreito through a new lightning incidence model based on the deflection of the electric field, which is sensitive to small variations of the electric potential on the structure's surface [22,23]. In this work, EFD model simulations are applied to the guyed tower topology used on the stretch between Belo Monte and Estreito through the finite element method, in 2D and 3D, using commercial software COMSOL Multiphysics®. The protection level of the LPS is to be assessed for the current positioning of the arrestor cables and also for a possible optimized configuration.

**Table 2.** Constructive characteristics Xingu - Estreito line. Adapted from [16].

Characteristics	Quantity/Measure
Nominal voltage	$\pm 800$ kV
Total length	2086.9 km
Conductors	6 conductors per pole, AC type, 1590 MCM
Right-of-way's width	100 m (Stretches 1 to 5—between Anapu (state of Pará) and Uruaçu (state of Goiás)) 110 m (Stretches 6 to 8—between Uruaçu and Ibiraci (state of Minas Gerais))
Estimated number of towers	3749
Span between towers	550 m (Stretches 1 to 5—between Anapu and Uruaçu) 560 m (Stretches 6 to 8—between Uruaçu and Ibiraci)
Tower characteristics	Guyed (80%) and Self-supporting (20%)
Site clearing area	Self-supporting: average of 2500 m <sup>2</sup> (50 m $\times$ 50 m) Guyed: average of 3000 m <sup>2</sup> (60 m $\times$ 50 m)

Lateral Distance (LD) and Shielding Failure Width (SFW) are analyzed as illustrated in Figure 1. Lateral distance is the longitudinal boundary width which contains the longest path. SFW is the longitudinal interval which contains the paths that reach the conductors (positive or negative) [24,25].

Corona effects were not taken into account as they present very short lengths, in the order of a few centimeters [26], and are considered therefore negligible in comparison to the average step length of lightning which is typically in the order of tens of meters [27].

**Figure 1.** Diagram that illustrates lateral distance (LD) and shielding failure width(SFW).

In the following section is given a description of the EFD model. In the materials and methods section is presented the boundary conditions used for the simulations, the tower's dimensions and the electrogeometric model that will be used as a reference for comparison between results. In the results section is presented the tower potentials with their respective values of electric field intensity and lightning strike distribution in 2D and 3D. Finally, in the last session is presented the conclusions reached from the analysis of the results obtained from both EFD and electrogeometric models.

## 2. Electric Field Deflection (EFD) Model

The first notions of Electric Field Deflection were recently presented in [22,23]. This model can be described as following:

Consider a conventionally uniform positive downward leader as in Figure 2. A positive leader is constituted of a leader tip, a leader channel and a streamer zone [27]. At the leader's tip, the potential over the point  $P$  is  $V$ . The downward leader leaps to point  $P'$  in the direction of the streamers of highest current intensity. The voltage drop can be obtained by Ohm's Law as

$$V - V' = Ri \quad (1)$$

where  $R$  is the impedance between points  $P$  and  $P'$ , admitted as purely resistive,  $i$  is the current intensity of the discharge.

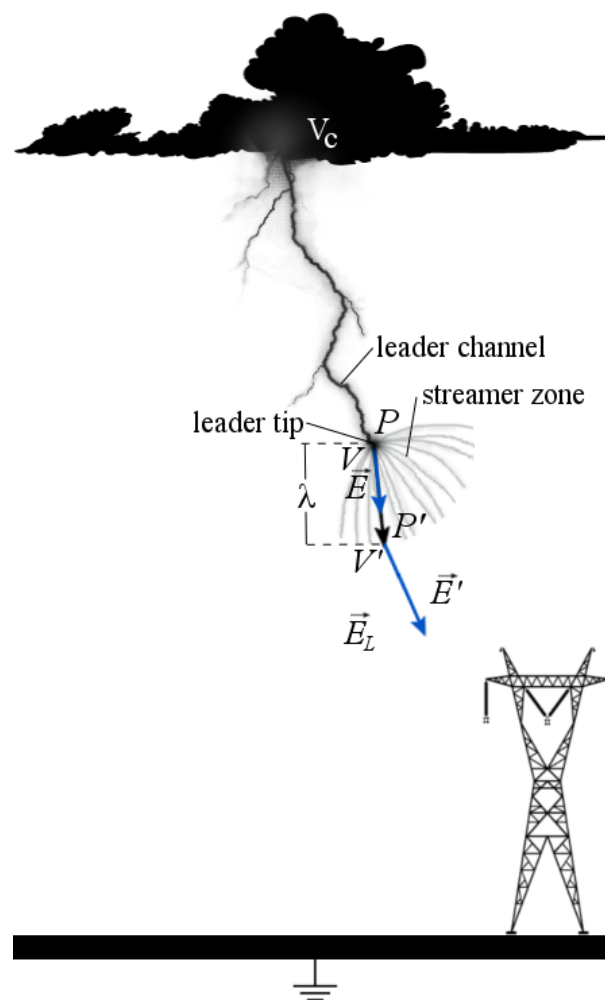


Figure 2. Diagram of the downward leader as described by the EFD.

According to Ohm's Second Law, the resistance is given as a function of the length ( $\lambda$ ), the leader channel's conductivity's ( $\sigma$ ) and the cross-sectional area ( $A$ ), and can be expressed as

$$R = \frac{\lambda}{\sigma A} \quad (2)$$

Substituting Equation (2) in Equation (1), we have

$$V - V' = \frac{\lambda}{\sigma A} i, \quad (3)$$

By obtaining the gradient of the function given by Equation (3), taking into account that the electric field vector is defined as being the negative gradient of the potential function, we have

$$-\vec{E} + \vec{E}' = \nabla \frac{\lambda i}{\sigma A} \quad (4)$$

where  $\vec{E}$  is the electric field at point P and  $\vec{E}'$  is the electric field at point P'.

According to the punctual form of Ohm's Law, the magnitude of the electric field can be described in function of the magnitude of the current density and the conductivity by

$$E = \frac{J}{\sigma}. \quad (5)$$

And the magnitude of the current density  $J$  can be given in terms of the ratio between the current intensity  $i$  and the cross-sectional area  $A$ , that is,

$$J = \frac{i}{A}. \quad (6)$$

Substituting Equation (6) in Equation (5)

$$E = \frac{i}{\sigma A}. \quad (7)$$

And substituting Equation (7) in Equation (4), considering that  $\lambda$  does not depend on direction and position, we have

$$\vec{E}' = \vec{E} + \lambda \nabla E \quad (8)$$

Equation (8) describes a discrete path of lightning in steps of length  $\lambda$ . However, if we compute a continuous leader movement, we would still obtain a path which is very similar to the non-ramified lightning, that is,

$$\vec{E}_L \approx \vec{E} + \lambda \nabla E \quad (9)$$

where  $\vec{E}_L$  represents the resulting electric field, which determines the direction of propagation of the lightning which accelerates the leader tip ( $q$ ) in continuous motion. In this case,  $\lambda$  represents the step length. The second term is referred to as electric field displacement term.

### 2.1. Dependence on Peak Current

The most widely used model for the design of air-termination systems of a transmission line is the Electrogeometric Model (EGM). The final version of the EGM was published in 1973 [21]. This model is based on the concept of striking distance ( $r_s$ ), which consists in estimating the distance between the last downward leader and the grounded structure. If this distance is smaller than a value  $r_s$ , it is assumed that the leader will strike the structure [28,29]. Brazilian standard NBR 5419 and also IEC 62305 [30,31] recommend

$$r_s = 10 I_p^{0.65} \quad (10)$$

In incidence models, there is interest in knowing the path of lightning primarily in the surroundings of the structures to be protected. The average step of the scaled leader is about 50 m [27]. Observing Table 3, it can be seen that this value is close to the striking distance value estimated by the electrogeometric models for lightning with peak current equal to 10.1 kA, which is

$r_s = 45$  m. For other current values, it is also considered that  $\lambda \approx r_s$ . Therefore, substituting Equation (10) into Equation (9), we obtain

$$\vec{E}_L \approx \vec{E} + 10I_p^{0.65} \nabla E \quad (11)$$

**Table 3.** Peak current and strike distance by protection levels [30,31].

Protection Level	Peak Current (kA)	Striking Distance (m)
I	2.9	20
II	5.4	30
III	10.1	45
IV	15.7	60

In this electrostatic model, it is assumed that the upward leader will trail through the field lines determined by Equation (11), starting at a point  $P$ .

The electric field  $\vec{E}$  is a function of the electric potential defined by

$$\vec{E} = -\nabla V. \quad (12)$$

And, in a non-homogenous medium, the potential can be obtained by solving the Poisson Equation, given by

$$\nabla \cdot (\epsilon \nabla V) = -\rho \quad (13)$$

where  $\epsilon$  is the electric permittivity of the medium.

### 3. Materials and Methods

Equations (11)–(13) were then solved through finite element method in two and three dimensions with aid of Comsol Multiphysics<sup>®</sup> software. All simulations were carried out either within a cubic (3D) or a square (2D) domain, both with edge of 250 m, as illustrated in Figure 3a. On the upper face of the cube, or on the upper edge of the square, the potential is defined as  $-12.5$  MV, while the lower face of the cube, or the lower edge of the square, is defined as null potential (ground). This difference of potential generates an electric field with intensity of  $50$  kV/m and is equivalent to the one generated by the flat base of a storm cloud with  $-100$  MV at a height of  $2$  km [29]. The positive potential on the upper face of the domain produces downward negative lightning to ground or to the HVDC transmission system. This potential was defined as negative because around  $90\%$  of cloud-ground discharges are negative [27].

The tower design included in the simulation is a HVDC  $800$  kV tower (Figure 3b). The tower structure and cables were considered as line segments with negligible thickness. The positive pole of the transmission tower was set at  $800$  kV, and the negative pole at  $-800$  kV.

The poles are located at a height of  $32.5$  m, suspended by cross arms with length of  $10.20$  m, as illustrated in Figure 3b. Two arrestor cables are located at a height of  $45.9$  m, above the positive and negative poles.

Figure 4 presents an analysis of the incidence of lightning strikes through electrogeometric model. The position of the arrestor cables and of the positive and negative pole were considered as given in Figure 3b. Through the electrogeometric model, it is assumed that lightning will strike the central points as they cross each circle arc. For strikes with parameters of level I ( $I_p = 2.9$  kA and  $r_s = 20$  m), the electrogeometric model indicates that the strikes might hit the positive and negative poles equally, hitting the line through  $22$  m arcs. For protection level II ( $I_p = 5.4$  kA and  $r_s = 30$  m), the arcs which lead to strikes at the poles are reduced to  $8$  m. For protection level III ( $I_p = 10.1$  kA and  $r_s = 45$  m), the arcs centered around the poles are inferior to  $1$  m. For level IV ( $I_p = 15.7$  kA and  $r_s = 60$  m), there are no indications of strike over the line. Thus, according to the electrogeometric



model, the original tower presents level IV protection. As this model is geometric, the potential of the poles of the lines ( $-800$  and  $800$  kV) are not taken into account, and the incidence of strikes would be symmetric.

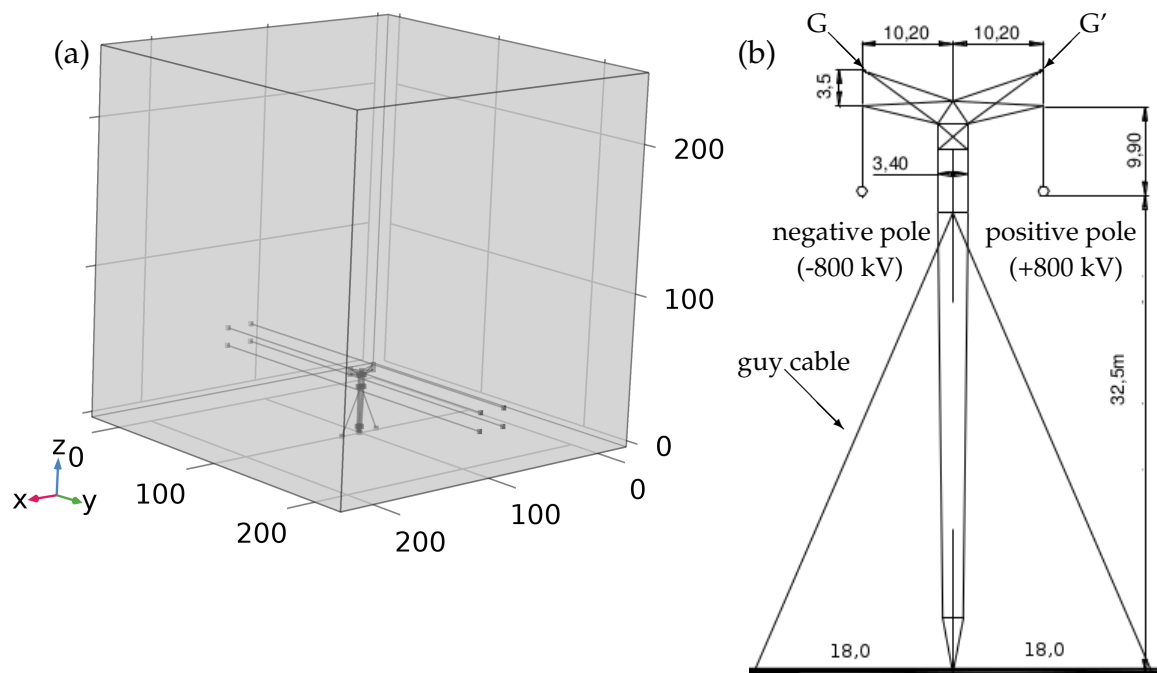


**Figure 3.** (a) Domains containing a HVDC line segment with a guyed tower. Coordinates  $x$ ,  $y$  and  $z$  are given in metres (b) Dimensions in metres of the guyed tower.  $G$  and  $G'$  are the arrestor cables.

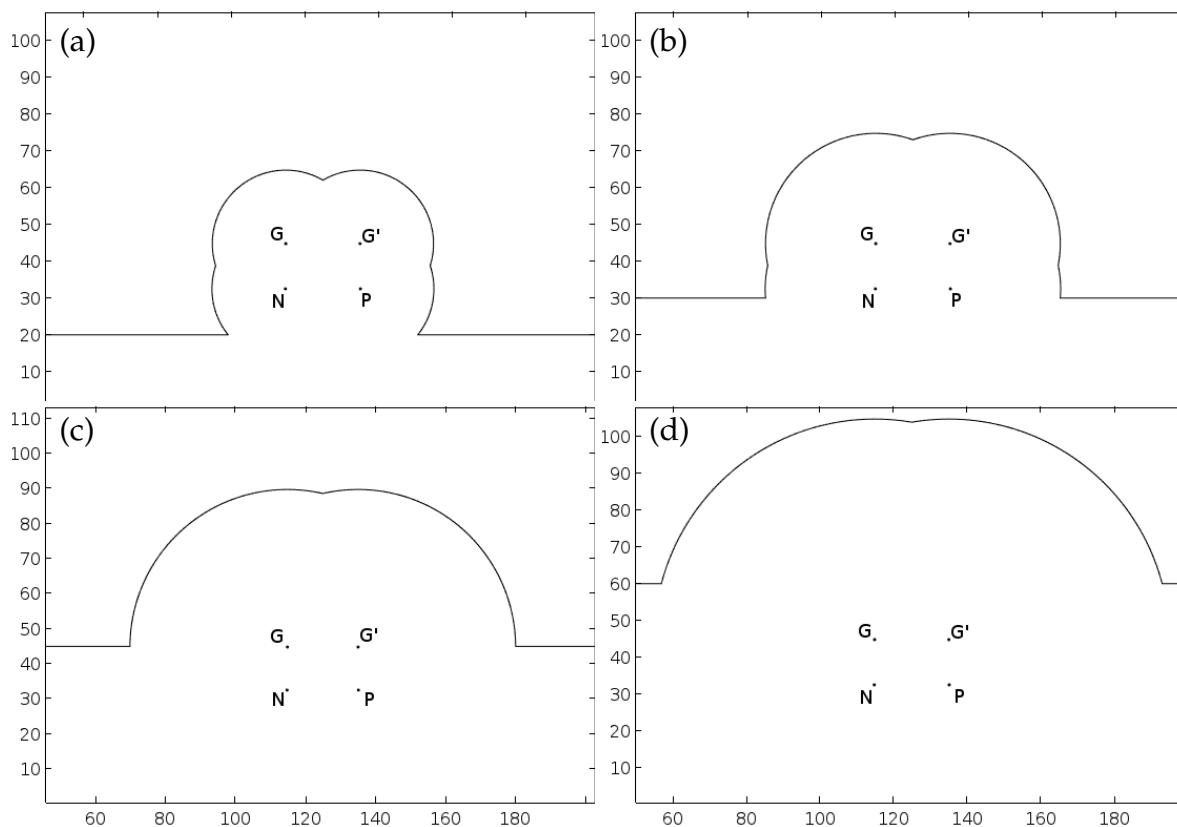


**Figure 4.** Analysis as given by the Electrogeometric Model on the span region of a conventional HVDC line topology. (a)  $I_p = 2.9$  kA, (b)  $5.4$  kA, (c)  $10.1$  kA and (d)  $15.7$  kA.



As about 90% of cloud-ground lightning are of negative polarity [27], the positive pole of the HVDC line is expected to attract more lightning than the negative pole. Thus, in this work we propose a rearranging of the positions of the arrestor cables in order to reduce shielding failure widths over the positive pole of the line, as illustrated in Figure 5. Figure 5a shows the line's transverse section plane in the span region for the conventional topology, while Figure 5b shows the proposed topology with cable G shifted 5 m and cable G' shifted 9 m in the positive direction of the  $x$ -axis. Both topologies were submitted to the lightning incidence analysis described in Section 2.

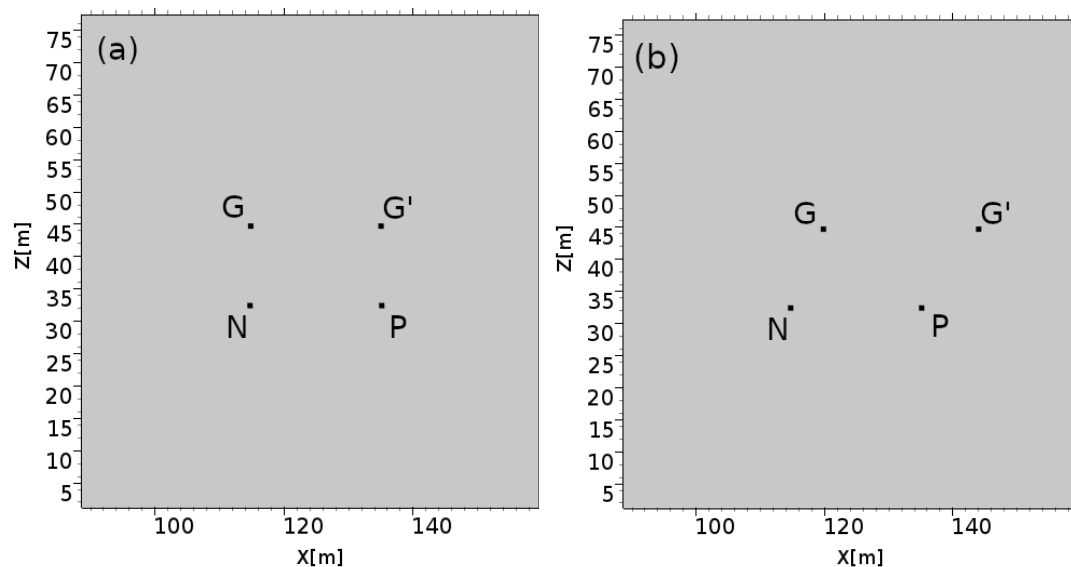


**Figure 5.** Cross-section of the HVDC line in the middle of the span region. G and G' indicate the positions of the arrestor cables. N and P indicate the positions of the negative and positive poles, respectively. (a) Conventional topology, (b) Proposed topology. Arrestor cable G was shifted 5 m in the positive direction of the  $x$ -axis, while arrestor cable G' was shifted 9 m in the same direction.

Through EFD's tridimensional analysis, 500 lightning are inserted uniformly at the upper face of the domain. A lightning's typical step length  $\lambda = 50$  m is used in Equation (9). The catenary curve of the line's cables was not taken into account. The variations in the permittivity of air were considered negligible. Thus,  $\epsilon \approx \epsilon_0$ .

EFD's two-dimensional analysis is done on two transverse planes: (i) the tower plane and (ii) in the the region of span between two towers, 125 m away from the tower. In each plane, 251 lightning are inserted equally spaced by 1 m in the upper segment. Four peak currents are analysed as defined by the protection levels in Table 3. The lateral distance (LD) and Shielding Failure Width (SFW) verified are presented in Figure 1. The four levels of current defined by standard IEC 62305 were presented in Table 3 and used in Equation (11). Overvoltages due to direct strikes (flashover) and indirect strikes (back-flashover) are not analyzed.

It is expected that most of lightning strike the arrestor cables. However, due to coulomb attraction, some lightning originated from cloud potentials that are negative in reference to earth strike the positive pole of the HVDC line, representing a shielding failure width which was not perceived through analyses by electrogeometric modeling. The results of these simulations are presented in Section 4.

#### 4. Results

Figure 6 illustrates the electric potential at the tower plane. It can be verified that the potentials at the poles are respectively  $-800$  kV (blue) and  $800$  kV (red). On the tower's structure, potential is null (green), as it is grounded.

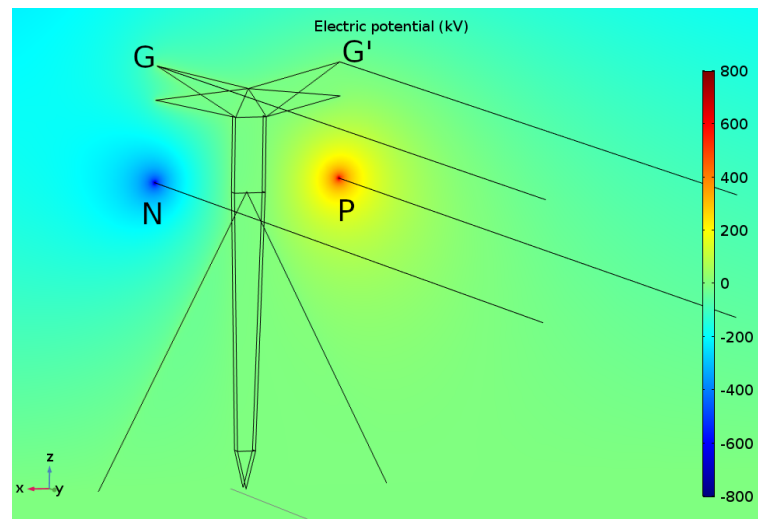


Figure 6. Electric Potential.

Figure 7 illustrates the electric field at the tower plane. In stormy weather conditions, air's dielectric strength is lower, between 100 and 500 kV/m, due to humidity. In the simulation of stormy weather conditions, the obtained electric field's intensity exceeds 300 kV/m, being able to generate a dielectric breakdown and therefore attract lightning to the transmission line.

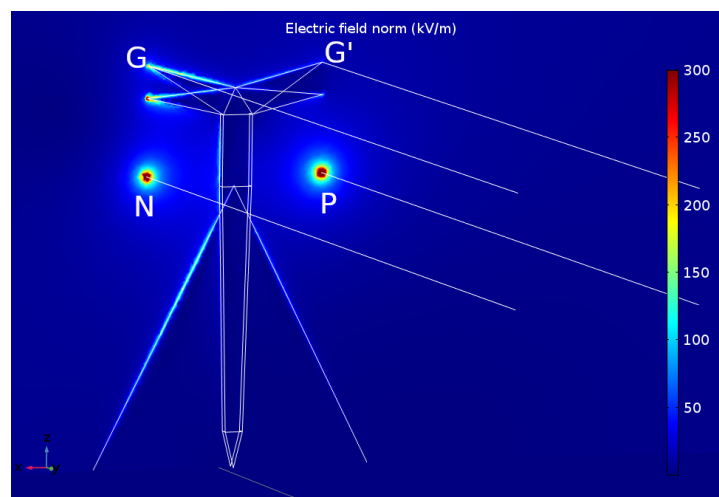


Figure 7. Electric field.

Through Equation (9) we can obtain the path of lightning as estimated by EFD method. Figure 8 presents the path of lightning (cyan lines) for  $\lambda = 50$  m. This is the typical step length value for lightning [27].

It can be seen from Figure 8 that the incidence of lightning does not change significantly along the line. The highest rates of discharge tend to hit the positive pole and, for this case, no lightning hits the negative pole. That can be explained by the fact that the simulated lightning are negative and therefore are repelled by coulomb interactions by same signal charges and attracted by opposite signal charges.

Figure 9a indicates that the distribution of lightning is different in the tower plane. Figure 9b shows that few lightning are attracted to the tower plane. Thus, the incidence analysis on the plane parallel to the lines can be discarded, and only the planes which are transverse to the lines are considered.

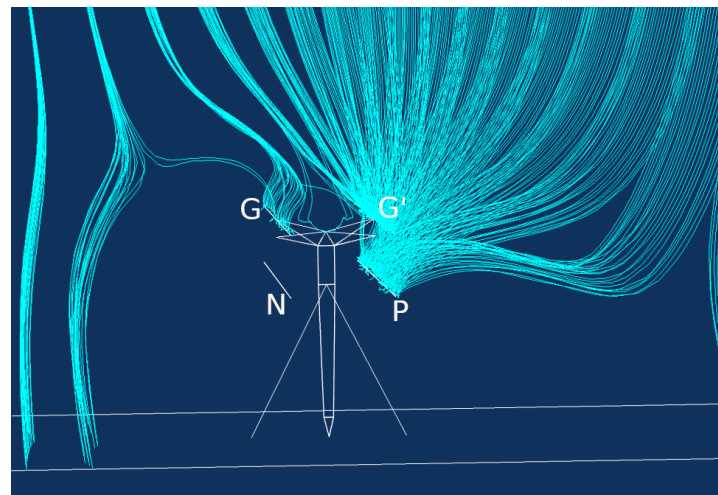


Figure 8. Lightning incidence (cyan lines) for  $\lambda = 50$  m.

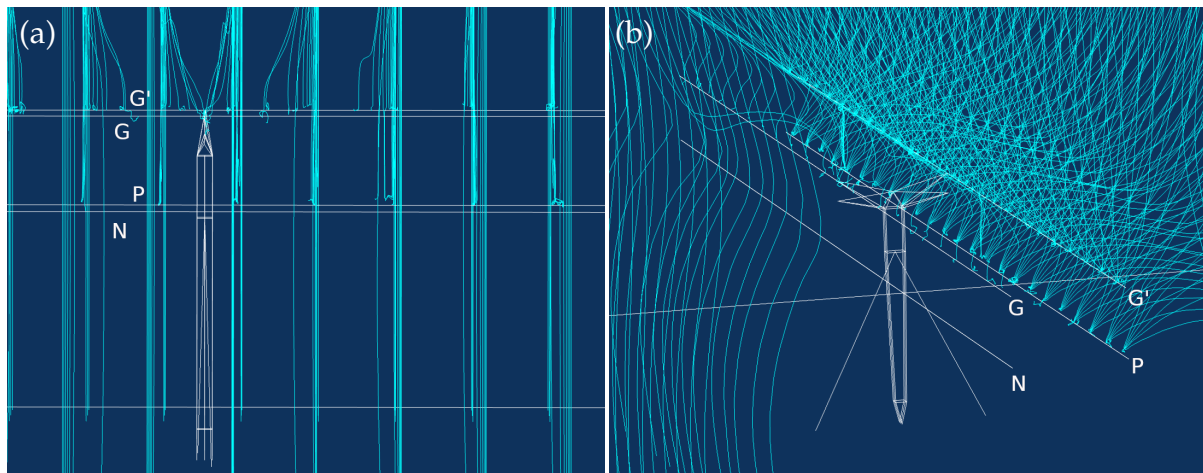


Figure 9. Lightning incidence (cyan lines) for  $\lambda = 50$  m: (a) Perspective view and (b) side view.

The lightning incidences on the tower plane and on the span are illustrated separately in Figures 10 and 11. The four levels of protection in Table 3 are analysed.

In the tower plane, for peak current ( $I_p$ ) of 2.9 kA (striking distance  $r_s = 20$  m), the lateral distances obtained in Figure 10a was 50 m, and the shielding failure width (SFW) was 9 m, on the positive pole side. These values represent the smallest lateral distance and the largest SFWs within the four protection levels. Due to the low current intensity, the charge build-up in the downwards leader is smaller, therefore the coulomb force is also smaller, which reduces the air-termination's efficiency.

For  $I_p = 5.4$  kA ( $r_s = 30$  m), lateral distance was increased to 59 m, while SFW was reduced to 4 m at the positive pole (Figure 10b). This was the only case in which there were lightning strikes on the negative pole, which presented SFW of 2 m. This small shielding failure on the positive pole can be attributed to the fact that the potential on the base of the cloud ( $-100$  MV) is still higher than the potential on the positive pole of the HVDC line ( $-800$  kV). Therefore, the difference of potential between the base of the cloud and negative pole can lead to a strike on the negative pole. The tower's guy cable, which is connected to ground, can also attract strikes from a distance and some of these strikes can have their trajectories deflected towards the pole, even though it is the negative one, due to the gradient of the modulus of the electric field in the second term of Equation (11).

For  $I_p = 10.1$  kA ( $r_s = 45$  m), lateral distance was increased to 69 m and no strike to any of the poles was observed Figure 10c). As the analysis was carried out by inserting strikes each 1 m of the domain, the shielding failure width is not larger than 1 m. In this case, it is considered that the line is protected.

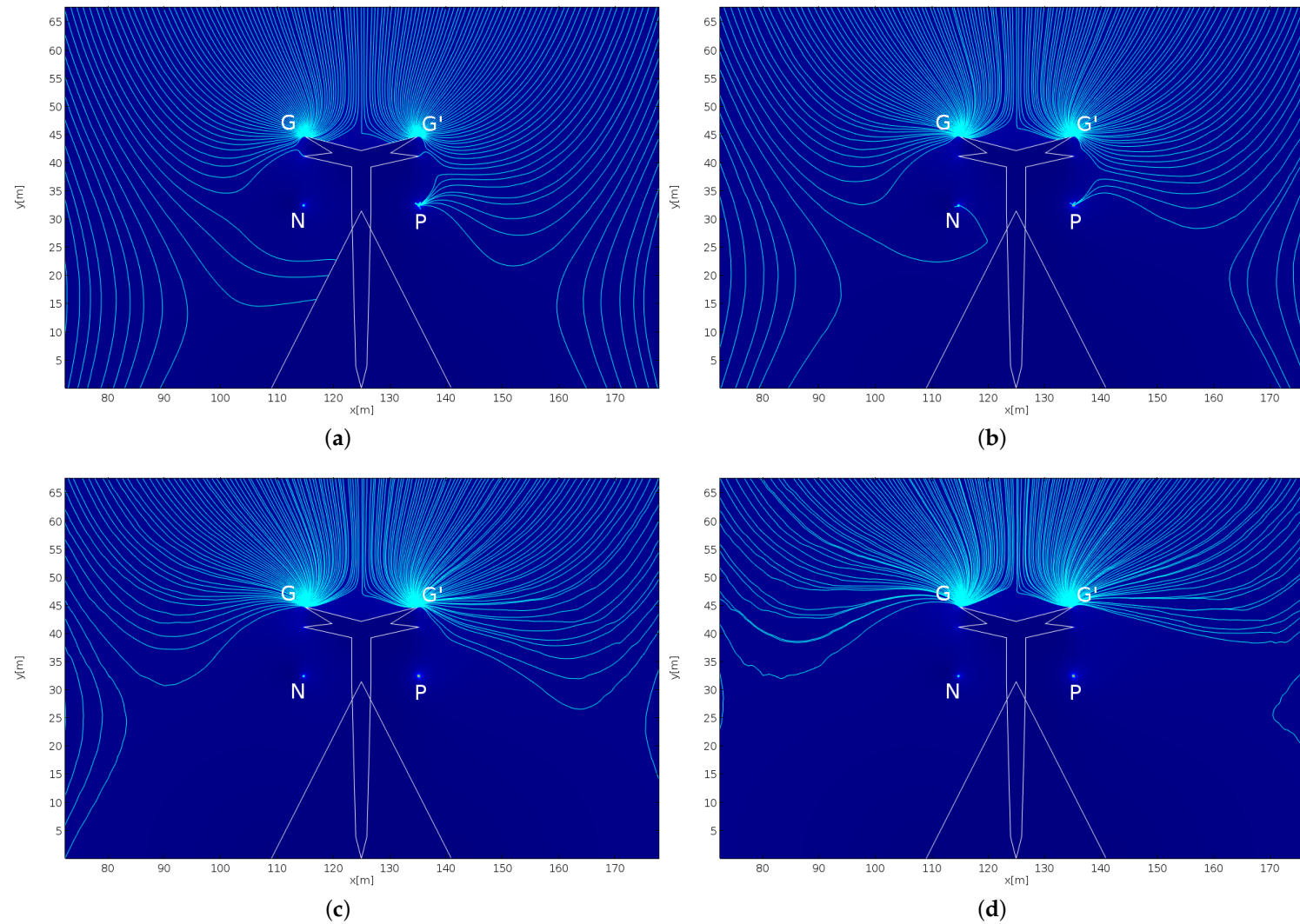


**Figure 10.** Lightning incidence on the tower plane as given by EFD model. (a)  $I_p = 2.9$  kA, (b) 5.4 kA, (c) 10.1 kA and (d) 15.7 kA.

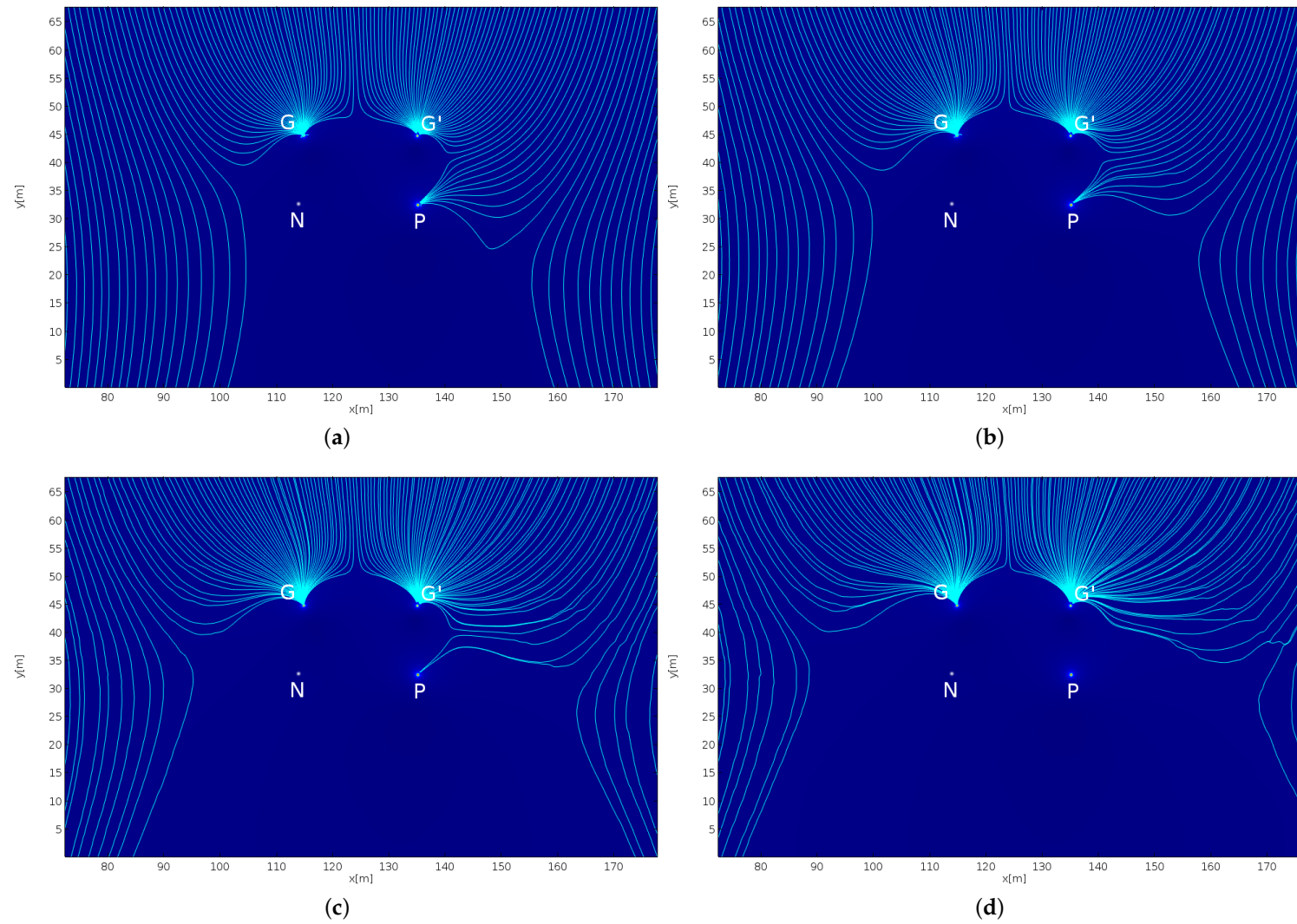


**Figure 11.** Lightning incidence in the span region as given by EFD model. (a)  $I_p = 2.9$  kA, (b) 5.4 kA, (c) 10.1 kA and (d) 15.7 kA.



For  $I_p = 15.7$  kA ( $r_s = 60$  m), LD was increased further to 73 m and no SFW was observed (Figure 10d).

In the span region, as illustrated in Figure 11, it can be seen that the positive pole tends to present higher chance of direct strike. In the simulation for  $I_p = 2.9$  kA, LD was 36 m. SFW was 12 m, representing an increase of 33 % for the same level in comparison to the one for the tower plane.

For  $I_p = 5.4$  kA, in spa region, there were no more direct strikes on the negative pole. That means the towers guy cable exerted an influence on the paths of the lightning, increasing the chances of direct strike on the pole. This type of result could not be noticed by means of geometric incidence models such as the electrogeometric model. LD for this case was 43 m and SFW on the positive pole was 8 m.

For  $I_p = 10.1$  kA, in the span region, LD was 54 m, and SFW was 4 m. For this same current, on the tower plane, there was no shielding failure with. This means that, in the span region, the line is more vulnerable to direct lightning strike.

For  $I_p = 15.7$  kA, in the span region, lateral distance was 63 m and no shielding failure was observed. Therefore, the topology in Figure 3b presents protection level IV.

The analyses have shown that the line is more vulnerable in the span region than in the tower plane. These analyses through EFD modeling indicate also that the positive pole is more subject to direct lightning strikes than the negative pole, given that cloud-earth lightning with negative charges are more frequent in nature.

In this work, we then proposed that the arrestor cables in HVDC transmission lines be no longer symmetrically positioned (Figure 5b). A simulation was then carried out with the arrestor cable (G) above the negative pole shifted 5 m toward the tower (negative direction of the  $x$ -axis in Figure 3b), and the one (G') above the positive pole shifted 9 m away from the tower (also negative direction of the  $x$ -axis in Figure 5b).

In this topology with the proposed modification, as shown in Figure 12a, a shielding failure occurred only for lightning with peak currents of 2.9 kA (Level I). Also, shielding failure width in the span region was reduced to 6 m. This represents a reduction of 50 % in the SFW on the positive pole (Figure 12a). The proposed topology, according to EFD Model simulation results, presents protection level II, as no direct strikes were observed for peak currents equal to or greater than 5.4 kA (Figure 12b–d). The original topology, illustrated in Figure 3b, presents protection level IV, which is the least rigorous among the four levels analysed (smallest efficiency).

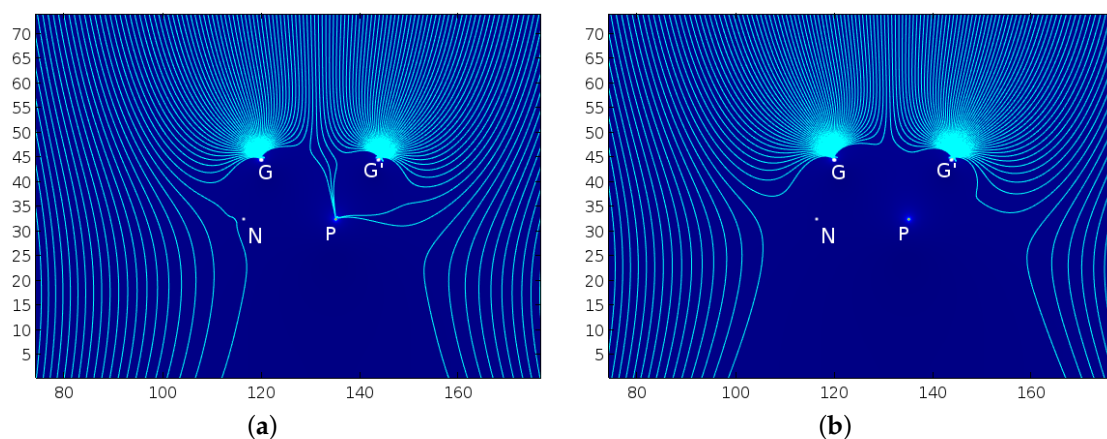
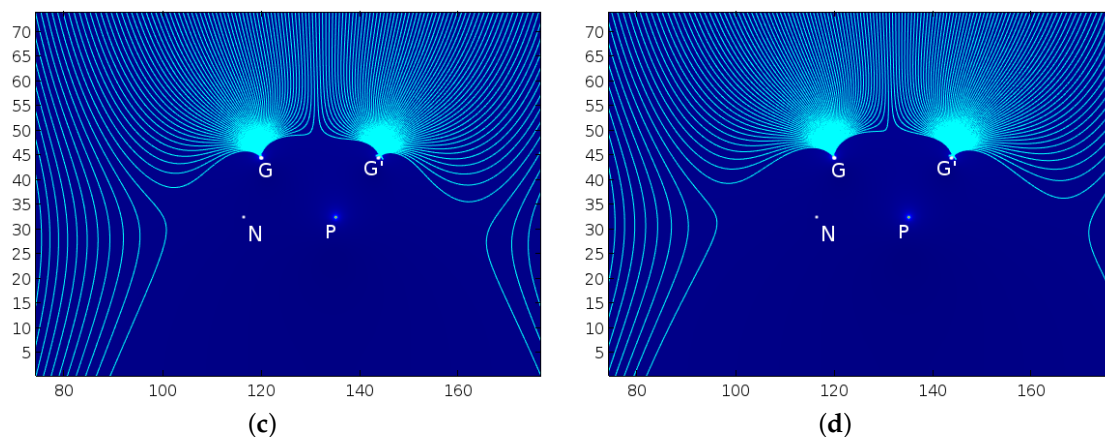


Figure 12. Cont.



**Figure 12.** Lightning incidence, as given by EFD Model, for the span region with proposed modifications. (a)  $I_p = 2.9$  kA, (b) 5.4 kA, (c) 10.1 kA and (d) 15.7 kA.

## 5. Conclusions

Geometric incidence models, like electrogeometric model, do not take into account the electric potentials in the transmission line cables. Therefore, the incidence analysis by means of this method tends to overestimate the protection zones of the LPS's in HVDC transmission lines.

The analysis by EFD indicate that the positive pole of the HVDC line is more vulnerable to direct strikes than the negative one, given that cloud-earth lightning with negative charges are the most frequent in nature. This method also indicated that the line is more vulnerable to strikes in the span region than in the tower plane.

The original, symmetric topology presented significant shielding failure widths as by EFD modelling in two planes which are transverse to the HVDC transmission line: the tower plane and the span region.

At the tower plane, the shielding failure widths were of 9 m and 2 m over the positive pole of the line for peak current of 2.9 and 5.4 kA, respectively. No shielding failure widths were observed for peak current of 10.1 and 15.7 kA on the tower plane.

In the span region, shielding failure widths were of 12 m, 8 m and 4 m for peak currents of 2.9, 5.4 and 10.1 kA, respectively, on the positive pole, which endorses the conclusion that the line is more vulnerable to direct strikes at the span region rather than near the tower.

It was proposed a spatial shifting of the arrestor cables (G and G' in Figure 5b) toward the region with largest shielding failure widths. The study pointed that shiftings of 5 m and 8 m for the arrestor cables above the negative (G) and positive (G') pole, respectively, reduced shielding failure width in 50 % for lightning with peak current of 2.9 A. For peak currents of 5.4, 10.1 and 15.7 kA, no shielding failure widths were observed for the topology with the proposed modification on the positioning of the arrestor cables above the HVDC line analysed.

**Author Contributions:** All authors have equivalent contributions to the development of the work.

**Funding:** This research received no external funding.

**Acknowledgments:** The authors thank FUNCAP for the financial support and CENAPAD for the use of high performance computers.

**Conflicts of Interest:** The authors declare no conflict of interest.

## References

1. Chou, C.; Wu, Y.; Han, G.; Lee, C. Comparative evaluation of the HVDC and HVAC links integrated in a large offshore wind farm—An actual case study in Taiwan. *IEEE Trans. Ind. Appl.* **2012**, *48*, 1639–1648. [\[CrossRef\]](#)



2. Meah, K.; Ula, S. Comparative evaluation of HVDC and HVAC transmission systems. In Proceedings of the 2007 IEEE Power Engineering Society General Meeting, Tampa, FL, USA, 24–28 June 2007; pp. 1–5. [CrossRef]
3. Chesney, C.C.; Scott, C.F. Early history of the A-C system in America. *Trans. Am. Inst. Electr. Eng.* **1936**, *55*, 228–235. [CrossRef]
4. Woodbury, E. 150,000-volt transmission system. *Trans. Am. Inst. Electr. Eng.* **1914**, *XXXIII*, 1283–1298. [CrossRef]
5. Dwight, H.B. Constant voltage transmission. *Proc. Am. Inst. Electr. Eng.* **1913**, *32*, 1357–1372. [CrossRef]
6. Tesla, N. A new system of alternate current motors and transformers. *Trans. Am. Inst. Electr. Eng.* **1888**, *V*, 308–327. [CrossRef]
7. Kimbrak, E.W. *Direct Current Transmission*; Wiley Interscience: New York, NY, USA, 1971.
8. Holm, J.G. Direct-current power transmission [includes discussion]. *Trans. Am. Inst. Electr. Eng. Part III Power Appar. Syst.* **1953**, *72*, 1114–1120. [CrossRef]
9. Rudervall, R.; Charpentier, J.P.; Sharma, R. High Voltage Direct Current (HVDC) Transmission Systems Technology. In Proceedings of the Energy Week 2000, Washington, DC, USA, 7–8 March 2000.
10. Lebre, J.R.; Portugal, P.M.M.; Watanabe, E.H. Hybrid HVDC (H2VDC) system using current and voltage source converters. *Energies* **2018**, *11*, 1323. [CrossRef]
11. EPE Brazilian Energy Balance. Available online: [epe.gov.br/pt/publicacoes-dados-abertos/publicacoes/balanco-energetico-nacional-2018](http://epe.gov.br/pt/publicacoes-dados-abertos/publicacoes/balanco-energetico-nacional-2018) (accessed on 4 January 2019).
12. ONS. Available online: <http://ons.org.br/> (accessed on 4 January 2019).
13. ITAIPU BINACIONAL. Available online: <https://www.itaipu.gov.br/> (accessed on 4 January 2019).
14. EPE 10–Year Energy Expansion Plan 2010–2019. Available online: <http://www.epe.gov.br/pt/publicacoes-dados-abertos/publicacoes/Plano-Decenal-de-Expansao-de-Energia-2019> (accessed on 4 January 2019).
15. NORTE ENERGISA. Available online: <https://www.norteenergisa.com.br/pt-br/uhe-belo-monte> (accessed on 4 January 2019).
16. BMTE Environmental Impact Assessment. Available online: <http://www.bmte.com.br/wp-content/uploads/2016/06/RIMA.pdf> (accessed on 4 January 2019).
17. INPE WebRaios. Available online: [http://www.inpe.br/webelat/ABNT\\_NBR5419\\_Ng/](http://www.inpe.br/webelat/ABNT_NBR5419_Ng/) (accessed on 4 January 2019)
18. Golde, R. *Lightning Protection*; Edward Arnold: London, UK, 1973.
19. Uman, A. *The Art and Science of Lightning Protection*; Cambridge University Press: Cambridge, UK, 2008.
20. Cooray, V. *Lightning Protection*; The Institution of Engineering and Technology: London, UK, 2009.
21. Gilman, D.; Whitehead, R. The mechanism of lightning flashover on high-voltage and extra-high voltage transmission lines. *Electra* **1973**, *27*, 65–96.
22. Rodrigues, E.; Pontes, R.; Fernandes Neto, T. Novel lightning incidence model based on the electric field gradient: 2d Electrostatic analyses. In Proceedings of the International Conference on Grounding and Earthing & 7 th International Conference on Lightning Physics and Effects, Porto de Galinhas, Brazil, 6–9 June 2016.
23. Rodrigues, E.; Pontes, R.; Fernandes Neto, T. Lightning incidence model based on the electric field gradient: 3D electrostatic analyses. In Proceedings of the IEEE CEFC 2016 Conference on Eletromagnetic Field Computation, Miami, FL, USA, 13–16 November 2016.
24. Deller, L.; Garbagnati, E. Lightning stroke simulation by means of the leader progression model. I. Description of the model and evaluation of exposure of free-standing structures. *IEEE Trans. Power Deliv.* **1990**, *5*, 2009–2022. [CrossRef]
25. Deller, L.; Garbagnati, E. Lightning stroke simulation by means of the leader progression model. II. Exposure and shielding failure evaluation of overhead lines with assessment of application graphs. *IEEE Trans. Power Deliv.* **1990**, *5*, 2023–2029. [CrossRef]
26. Riba, J.; Morosini, A.; Capelli, F. Comparative study of AC and positive and negative DC visual corona for sphere-plane gaps in atmospheric air. *Energies* **2018**, *11*, 2671. [CrossRef]
27. Rakov, V.; Uman, M. *Lightning: Physics and Effects*; Cambridge University Press: Cambridge, UK, 2003.
28. Lee, R. Lightning protection of buildings. *IEEE Trans. Ind. Appl.* **1979**, *IA-15*, 236–240. [CrossRef]
29. Visacro, S. *Descargas Atmosféricas: Uma Abordagem De Engenharia*; Artliber: Sao Paulo, Brazil, 2005.

30. IEC—International Electrotechnical Commission. *IEC 62305 Series—Protection Against Lightning*, 2nd ed.; Furse: Nottingham, UK, 2010.
31. ABNT—Associação Brasileira de Normas Técnicas. *ABNT NBR 5419—Proteção de Estruturas Contra Descargas Atmosféricas*; Associação Brasileira de Normas Técnicas: Rio de Janeiro, Brazil, 2015. (In Portuguese)



© 2019 by the authors. Licensee MDPI, Basel, Switzerland. This article is an open access article distributed under the terms and conditions of the Creative Commons Attribution (CC BY) license (<http://creativecommons.org/licenses/by/4.0/>).